Journal of Marine Systems 139 (2014) 348–361

Contents lists available at ScienceDirect

Journal of Marine Systems

journal homepage: www.elsevier.com/locate/jmarsys

Modeling the biogeochemical seasonal cycle in the Strait of Gibraltar

E. Ramírez-Romero [a,1,*], M. Vichi [b], M. Castro [c], J. Macías [c], D. Macías [d], C.M. García [a], M. Bruno [e]

[a] Departamento de Biología, Área de Ecología, Facultad de Ciencias del Mar y Ambientales, Universidad de Cádiz, Cádiz, Spain
[b] Centro Euro-Mediterraneo sui Cambiamenti Climatici, Bologna, Italy
[c] Departamento de Análisis Matemático, Universidad de Málaga, Málaga, Spain
[d] European Commission, Joint Research Center, Institute for Environment and Sustainability, Via E. Fermi 2749, 21027, Ispra, Italy
[e] Departamento de Física Aplicada, Facultad de Ciencias del Mar y Ambientales, Universidad de Cádiz, Cádiz, Spain

ARTICLE INFO

Article history:
Received 16 October 2013
Received in revised form 22 May 2014
Accepted 18 July 2014
Available online 24 July 2014

Keywords:
Strait of Gibraltar
Tidal mixing
Biogeochemical patterns
Atlantic Inflow
Alboran Sea

ABSTRACT

A physical-biological coupled model was used to estimate the effect of the physical processes at the Strait of Gibraltar over the biogeochemical features of the Atlantic Inflow (AI) towards the Mediterranean Sea. This work was focused on the seasonal variation of the biogeochemical patterns in the AI and the role of the Strait; including primary production and phytoplankton features. As the physical model is 1D (horizontal) and two-layer, different integration methods for the primary production in the Biogeochemical Fluxes Model (BFM) have been evaluated. An approach based on the integration of a production-irradiance function was the chosen method. Using this Plankton Functional Type model (BFM), a simplified phytoplankton seasonal cycle in the AI was simulated. Main results included a principal bloom in spring dominated by nanoflagellates, whereas minimum biomass (mostly picophytoplankton) was simulated during summer. Physical processes occurring in the Strait could trigger primary production and raise phytoplankton biomass (during spring and autumn), mainly due to two combined effects. First, in the Strait a strong interfacial mixing (causing nutrient supply to the upper layer) is produced, and, second, a shoaling of the surface Atlantic layer occurs eastward. Our results show that these phenomena caused an integrated production of 105 g C m^{-2} $year^{-1}$ in the eastern side of the Strait, and would also modify the proportion of the different phytoplankton groups. Nanoflagellates were favored during spring/autumn while picophytoplankton is more abundant in summer. Finally, AI could represent a relevant source of nutrients and biomass to Alboran Sea, fertilizing the upper layer of this area with 4.95 megatons nitrate $year^{-1}$ (79.83 gigamol $year^{-1}$) and 0.44 megatons C $year^{-1}$. A main advantage of this coupled model is the capability of solving relevant high-resolution processes as the tidal forcing without expensive computing requirements, allowing to assess the effect of these phenomena on the biogeochemical patterns at longer time scales.

1. Introduction

The Strait of Gibraltar is the only connection between the Mediterranean Sea and the Atlantic Ocean. The water exchange between these two basins occurs following a two-layer, inverse-estuarine circulation scheme, with a mixture of Surface Atlantic Water (SAW) and North Atlantic Central Water (NACW) entering the Mediterranean Sea at surface and denser deep Mediterranean water outflowing towards the Atlantic (MOW). The intense hydrodynamics of the Strait can be considered the most important forcing agent explaining the distribution and behavior of biogeochemical variables in the Atlantic Jet (AJ) (e.g. Macías et al., 2007). The hydrological processes in the Strait, as in other coastal regions, cover a wide range of temporal scales including interannual, seasonal, sub-inertial and tidal (Lacombe and Richez, 1982). Thus, biological features in the Strait, heavily dependent on the physical processes, should follow these temporal scales too. In spite of the wide scales associated to the physical-biological coupling in the area, most of the studies have been focused on the tidal scale and particularly on internal waves generation and effects; e.g. biogeochemical effects of the undulatory processes currents have been widely studied (e.g. Macías et al., 2006; Vázquez et al., 2009). These relevant undulatory processes are forced by the interactions of sharp topography (Camarinal Sill) with tidal currents (e.g. Bruno et al., 2002).

The Atlantic Inflow (AI) through the Strait consists mainly of open ocean waters coming from the Gulf of Cádiz (Criado-Aldeanueva et al., 2006) with oligotrophic features (Macías et al., 2008; Navarro et al., 2006; Ramírez-Romero et al., 2012). Previous works showed that the pelagic ecosystem in the Gulf of Cadiz and near the open Atlantic

* Corresponding author at: Facultad de CC de Mar y Ambientales, Avda, República Saharaui sn, 11510 Puerto Real, Cádiz, Spain. Tel.: +34 956016024, +49 431 600 4411; fax: +34 956016019.
E-mail addresses: Eduardo.ramirez@uca.es, eramirez-romero@geomar.de (E. Ramírez-Romero).
[1] Present address: GEOMAR Helmholtz Centre for Oceanography, Düsternbrooker Weg 20, D-24105 Kiel, Germany.

http://dx.doi.org/10.1016/j.jmarsys.2014.07.017
0924-7963/

presents an annual cycle (Longhurst, 1995; Navarro and Ruiz, 2006; Navarro et al., 2012; Teira et al., 2005). The original seasonal cycle of biological features in the AI could, however, suffer important changes crossing the Strait. This modification is especially obvious during spring tides and includes interfacial mixing associated to internal waves or intrusions of high chlorophyll patches (Macías et al., 2006; Ramírez-Romero et al., 2012; Vázquez et al., 2009).

Assessment of phytoplankton productivity in the ocean is a key goal of Biological Oceanography, as assimilation of Carbon by marine phytoplankton via primary production is the basis of the ocean's food web and of the biological carbon pump. Hence, the determination of primary production rates is a relevant aim; however the complexity of the interactions of hydrodynamics with primary producers in the Strait constitutes a limitation but also an extra-motivation in this field laboratory. Classical incubation methods as oxygen evolution or C^{14} uptake (Macías et al., 2009) have already been used to estimate primary production in this area. Fluorescence-based measurements of photosynthesis have also been used in the area (Fast Repetition Rate Fluorometry, FRRF) (Bartual et al., 2011). Recent works have shown that biological probes (as FRRF) can be a useful tool to obtain high spatial and temporal resolution primary production estimations, particularly in highly dynamic systems (Bartual et al., 2011). Nevertheless, the non-synoptic and scattered nature of the sampling process implies limited spatial and temporal estimations of primary production, especially at larger scales as seasonal or interannual.

Coupled physical-biological models can cover these larger scales, including long-time processes and regional (e.g. Franks and Chen, 2001; Lazzari et al., 2012) or global scale simulations (Vichi et al., 2007a). In addition, due to its high spatio-temporal resolution, coupled models could cover a wide range of processes, as very local or short-scale could be simulated too. Nevertheless in the Strait, most of the modeling efforts focused on hydrodynamic processes (e.g. Izquierdo et al., 2001; Sánchez-Garrido et al., 2011; Sannino et al., 2007). Some studies included coupled physical-biological models (Macías et al., 2007; Skliris and Beckers, 2009). However, nitrogen-based, single compartments models, as used in previous works, did not provide direct estimations of C-based primary production nor of plankton's structure. In order to fulfill these aims, in the present work the Biogeochemical Flux Model (BFM) was used. This model distinguishes three different functional groups of phytoplankton (diatoms, nanoflagellates and picophytoplankton; see details in Vichi et al., 2007b). Furthermore, this model can simulate separately the dynamics for the C, N, P, Si and chlorophyll content; reproducing in a coarse way the physiological features of the different phytoplankton species. Therefore, BFM allows to infer the effect of the physical forcing on the different components of the model both under the taxonomic-biological and biogeochemical point of view.

The main purpose of this work was the development of a coupled model focusing in local phenomena at the central channel of the Strait of Gibraltar. As explained above, this is a very particular and extreme ecosystem forced by tidal dynamics. A proper inclusion of these local phenomena is needed to simulate correctly the processes in the Mediterranean basin (Malanotte-Rizzoli et al., 2013; Oguz et al., 2013; Sannino et al., 2009). To fulfill this aim, we propose a phytoplankton seasonal cycle, which could be used as an input or boundary condition for coupled models of the Mediterranean Basin. Our first aim was to simulate primary production and phytoplankton's biomass and structure in the incoming Atlantic waters (open ocean waters of the Gulf of Cadiz and nearby areas). Afterwards we assessed the effect of the hydrological processes (tidal forcing) at the Strait and their modulation of the biological features of the AI.

2. Methodology

2.1. Hydrodynamical model

The hydrodynamical component of the physical-biological coupled model was a 1-D two-layer shallow water model for channels with irregular geometry, in both width and depth. In this model sea-water density was uniform and prescribed in each layer. The first layer represented the surface Atlantic water entering the Alboran Sea, where biological processes take place. The second layer represented the denser Mediterranean water flowing deeper. A simple scheme of the model geometry is presented in Fig. 1, where A_1 and A_2 were the upper and lower layer wet area (depending on the position along the Strait axis and time)(Fig. 1a). h_1 and h_2 were the upper and lower layer thickness, respectively (Fig. 1b). A complete model description, including governing equations and parameter values used can be found in Castro et al. (2004a, b, 2009) and Bruno et al. (2010).

Model equations were discretized using a second order extension of the finite volume scheme presented in Castro et al. (2004a) by means of a flux limiter function as described in Toro (1989).

The biological model was a subset of the BFM (Vichi et al., 2007b) formulated in conservative form. The temporal changes in the concentration of the constituents were given by the general equation:

$$\frac{\partial(A_1\,C)}{\partial t}+\frac{\partial(u_1\,A_1\,C)}{\partial x}=\text{Biological terms};\tag{1}$$

where C was the concentration of a biogeochemical variable and u_1 was the upper layer averaged velocity.

2.1.1. Interfacial mixing between layers

Besides advection, interfacial mixing in the Strait of Gibraltar is a crucial phenomenon for understanding the biogeochemical patterns in this area (e.g. Macías et al., 2007). The value of the stability Froude number was used to determine interfacial mixing in order to avoid complex parameterizations strongly dependent on poorly constrained coefficients:

$$F_I^{\,2}=\frac{(u_1-u_2)^2}{g'\,(h_1+h_2)};\tag{2}$$

In this expression, u_1 and u_2 were the upper and lower layer averaged velocities, respectively. $g' = g\,(1 - r)$ was the reduced gravity with $r = \frac{\rho_1}{\rho_2} = \frac{1027}{1029} = 0.99805$ the ratio of densities, and g gravity.

When $F_I^2 > 1$, Kelvin-Helmholtz instabilities appear. In this situation, interfacial mixing has an important role (Cushman-Roisin, 1994). Then in a more complete form, biological flux equations were finally computed as:

$$\frac{\partial(A_1\,C)}{\partial t}+\frac{\partial(u_1\,A_1\,C)}{\partial x}=\text{Biological terms}\;+\;C_m;\tag{3}$$

where C_m was the mixing term, parameterized as:

$$C_m=k_{mix}*\left(C_{ref}-C\right);\tag{4}$$

$$k_{mix}=\alpha*F_I^2*A_1/h_1;\tag{5}$$

where k_{mix} was a function of the mixing between layers that parameterized as a function of the Froude stability number. C_{ref} was the constant concentration in the deep Mediterranean layer and C was the computed concentration of a variable for the upper Atlantic layer. α was a coefficient found calibrating this term with *in situ* data as explained below (here $\alpha = 0.002$). Therefore using this parameterization, mixing is proportional to F_I^2. Eq. (4) was valid for the physical variables (salinity, temperature) and biogeochemical variables with non-null concentration in the deep layer (Mediterranean layer) as nutrients. For the rest of the variables, mixing term was computed as: $C_m = -\,k_{mix}\,{}^{*}\,C$. The values for the variables in deeper layer have been collected in Table 1.

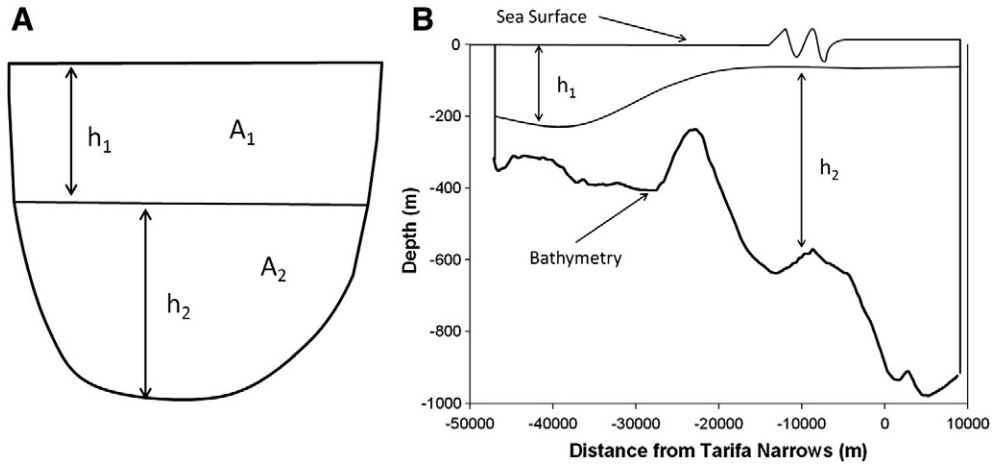

Fig. 1. Scheme and geometry of the model, showing the notations for a cross-section (A) and longitudinal section (B).

2.1.2. Coupling model components

The discretization of the BFM equations was performed in a fully coupled way with the hydrodynamical component, following the same procedure as Fernández-Nieto and Narbona-Reina (2008). In this method a flux limiter function was used to ensure the second order accuracy in space and time. It is worth to notice that here we did not use the so-called off-*line mode* in order to couple model components as the hydrodynamical numerical mass flow of the finite volume scheme is used in the definition of numerical flux for the biological component finite volume discretization. The coupled model had a variable time-step depending on CFL stability condition, approximately 5 s. The domain was divided in 200 sections, meaning a spatial resolution of 280 m. As an advantage of this kind of model, the performance of the simulation was not excessively expensive e.g. for one year of simulation, the model spent around 10 h.

2.1.3. Observational data

Data were collected during a cruise carried out in September 2008 on board the research vessel B/O "Sarmiento de Gamboa". One fixed station ("A" in the Tarifa Narrows, Fig. 2) was sampled twice during a period of approximately 24 hours. Collected data at station A (Fig. 1, narrowest section) can be considered representative of this whole section of the Strait, because this section has a quasi-rectangular shape with narrow coastal platforms and steep slopes (Fig. 1).

At this fixed station "A" (Fig. 2), several hourly CTD profiles were made using a combined CTD probe (Seabird SBE-911). Salinity was sampled from the surface to a depth of 200 m to mark the physical structure of the water column and the distribution of the water masses to be used in model validation. The depth of the Atlantic Mediterranean Interface (AMI) was associated with the 37.5 isohaline and the salinity of the surface layer was estimated as the average without taking into account the presence of NACW. Consequently, original salinity in the Atlantic layer was considered to be 36.5. Salinity values lower than 36.5 were replaced by a constant value of 36.5.

Table 1
Fixed values of the different variables in the deep layer and sources.

Variable	Value (deep layer)	Source
Nitrate (μM)	9.8	Macías et al. (2007)
Ammonium (μM)	1	own data
Silicate (μM)	8	own data
Phosphate (μM)	0.5	Huertas et al. (2012)
Temperature (°C)	13	Gascard and Richez (1985)
Salinity	38.4	Gascard and Richez (1985)

2.2. Biological model: Integrating primary production in a layer of variable depth

The original parameterisation used in the BFM considers that biological variables and rates are homogeneous over a layer of given constant depth, assuming that the upper water-column physical structure is adequately resolved with several levels of sufficiently small depths. However, in order to couple the BFM with the simplified hydrological model described above, biological parameterisations that are conceived for a level-explicit model had to be transformed into integrated single-layer functional responses. Specifically, we analysed the implementation of Integrated Primary Production (IPP) in a single-layer of variable depth (h_1, Fig. 1) and the implication of this parameterisation on phytoplankton physiology. This issue was already treated in some of the first coupled biological models of the mixed layer (e.g. Ebenhoh et al., 1997; Evans and Parslow, 1985; Fasham et al., 1990).

In this work, only the BFM equations for phytoplankton were implemented (chlorophyll, carbon and nutrients equations) and no grazing terms besides linear mortality have been included. Three standard functional groups are considered, diatoms, nanoflagellates and picophytoplankton. In the BFM (Vichi et al., 2007b), gross primary production (Gpp) is defined as:

$$Gpp = f_t * f_E * r_0 * P_C; \quad (6)$$

where f_t and f_E are the regulating factors for temperature and light respectively, both non-dimensional (0-1), r_0 the maximum potential specific photosynthetic rate and P_C is the phytoplankton carbon concentration. The light-regulating factor (f_E) considers the light environment in the layer; therefore it was integrated between surface ($z = 0$) and the bottom of the layer ($z = h_1$). Irradiance decays exponentially with depth, depending on the concentration of chlorophyll (self-shading effect) and the coefficient of attenuation of pure water. Two ways of computing integrated primary production were considered:

(i) Mean Irradiance Production (MIP): the exponential-decay curve of the light was integrated between the boundaries of the layer, in order to obtain the averaged irradiance of the layer and the resulting primary production. Light equation, as function of depth, is defined as:

$$E(z) = E_0 * \exp(-(\lambda_0 + \lambda_{Chla} * P_l)z); \quad (7)$$

where P_l is the phytoplankton chlorophyll concentration. We define $\lambda = (\lambda_0 + \lambda_{Chla} * P_l)$, where λ_0 is the coefficient

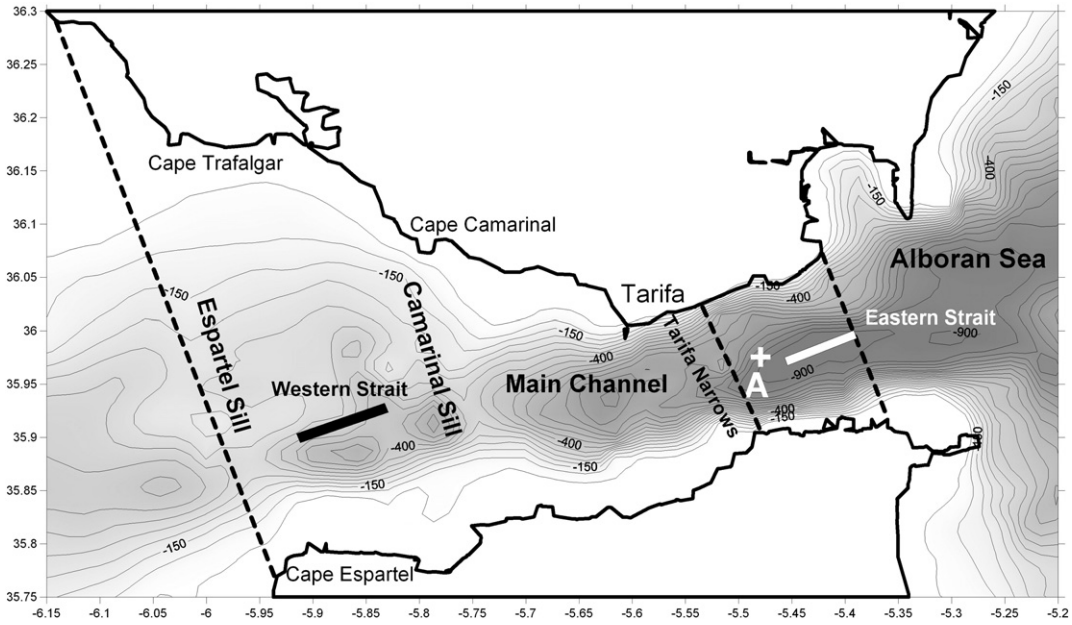

Fig. 2. Map showing the location, main geographic points of the study area and boundaries of the model. First and last sections of the model are marked with broken lines. The origin of longitudinal axes is marked with the central broken line (Tarifa Narrows). "A" marks the location of the fixed sampling station referenced in the text. Thick lines mark the central position of the Western Strait nodes (black) and Eastern Strait nodes (white).

of attenuation of pure water and λ_{chla} is the specific attenuation coefficient of chlorophyll. The average light in the layer ($\overline{E}$) is computed as:

$$\overline{E} = \frac{1}{h_1}\int_{h_1}^{0} E(z)dz = \frac{E_0}{\lambda^* h_1}(1-\exp(-\lambda^* h_1)); \quad (8)$$

Finally, this averaged light ($\overline{E}$) is transformed in the average light-regulating factor ($f_{\overline{E}}$) using a Production-Irradiance relation (P-E curve) (Platt et al., 1990; using notation from Sakshaug et al., 1997):

$$f_{\overline{E}} = 1-\exp(-\overline{E}/E_k);. \quad (9)$$

E_K is the light saturation parameter, calculated as $E_k = P_m/\alpha$ where P_m is the maximum chlorophyll-specific photosynthetic rate and α is the maximum light utilization coefficient. P_m is computed as $P_m = f_t * r_0 * P_C/P_l$. Then $\alpha = f_t * \alpha_0$, where α_0 is the potential maximum slope of the P-E curve. All these parameter and corresponding values were widely described in Vichi et al. (2007b). After some algebra, finally f_E becomes:

$$f_{\overline{E}} = 1-exp\left(-\frac{\alpha_0 * \overline{E} * P_l}{r_0 * P_C}\right); \quad (10)$$

(ii) Integrated Mean Production (IMP): This method considers production as a continuous function of depth and therefore implies the integration of a P-E curve between the boundaries of the layer. The chosen form of the P-E curve is the "ramp" or step function (Ebenhoh et al., 1997), which is simple enough to allow analytical solutions but provides a similar behaviour of more complicated functions with integro-exponential solutions. Following Ebenhoh et al. (1997), let p(E (z)) be the productivity per volume, then the light-dependent factor (f_E), as a function of surface irradiance E_0, in the considered layer of thickness h_1 (Fig. 1) is:

$$\overline{f_E} = \int_{h_1}^{0} p\left(E_0 * e^{-\lambda * z}\right) dz = \frac{1}{\lambda^* h_1}\int_{E_1}^{E_0}\frac{p(E)}{E}dE; \quad (11)$$

where E_1 is the light at the lower boundary of the layer ($z = h_1$), $E_1 = E_0 * \exp(-\lambda * h_1)$. P-E curve is defined as a simple ramp, in this way:

$$p(E) = p_0 * \min(1, x) \quad (12)$$

where $x = \frac{E}{E_k}$. p_0 is the maximum productivity value at optimal light; if $x = 1$, $p = p_0$ and $f_E = 1$. For the further calculation, it is useful to work with a dimensionless form of the ramp function q(x) as suggested by Ebenhoh et al. (1997):

$$q(x) = \min\left(\frac{1}{x}, 1\right); \quad \int q(x)dx = \begin{cases} 1 + \ln x & x>1 \\ x & x<1 \end{cases}; \quad (13)$$

and p(E) may be rewritten as:

$$p(E) = p_0 * x * q(x); \quad (14)$$

Using the function q(x) the depth integral can be expressed as:

$$\overline{f_E}(E_0) = \frac{p_0}{\lambda^* H}\int_{x_{h1}}^{x_0} q(x)dx; \quad (15)$$

where $x_0 = E_0/E_k$. And $x_1 = E_1/E_k = E_0/E_k * \exp(-\lambda * h_1)$. Finally, the application of the integral boundaries from Eqs. (14) and (15) leads to:

$$\overline{f_E} = \begin{cases} 1 & x_1 \geq 1; \\ \frac{1}{\lambda * h_1} * (\ln(x_0) + 1 - x_{h1}) & x_0 \geq 1 \\ \frac{1}{\lambda * h_1} * (x_0 - x_{h1}) & x_0 < 1; \end{cases}; \quad (16)$$

2.2.1. Effect of the layer's thickness on the integrated primary production

In order to assess the effect of a varying thickness of a single-layer on the integrated primary production, several set of simulations were done, using both of the proposed methods (MIP and IMP, Section 2.2). Therefore, integrated daily primary production (IDPP) was simulated in a set of 0-D numerical experiments varying the thickness of the layer and using different trophic environments. All simulations where

Table 2
Values of forcing factors and initial values of state variables used for the 0D set of simulations in the "oligotrophic" and "eutrophic conditions".

Conditions	"Oligotrophic conditions"	"Eutrophic conditions"
Integrated chlorophyll (mg m^{-2})	20	100
% diatoms/nanoflagellates/picophytoplankton	33:33:33	33:33:33
Initial C/Chl ratio	50	50
Temperature (°C)	18	18
Maximum surface irradiance (W m^{-2}) (I_0)	300	300
Nitrate (μM)	0.2	5
Phosphate (μM)	0.1	0.5
Silicate (μM)	0.1	8
Ammonium (μM)	0.00001	0.00001

done with the standard set of parameters of the BFM for the global ocean (see supplemental table in Vichi and Masina, 2009 for a list of values). "Oligotrophic" and "eutrophic conditions" were obtained from published data (Lorenzo et al., 2005; Marañón et al., 2003; Navarro et al., 2006; Teira et al., 2005) and are collected in Table 2. Nutrient concentrations were maintained constant in each numerical experiment until steady states have been reached (100 days). The resulting internal ratios were stored (C/Chlorophyll, C/N, C/P, C/Si) and the simulation was started again with constant nutrients for one day to estimate the Integrated Daily Primary Production (IDPP).

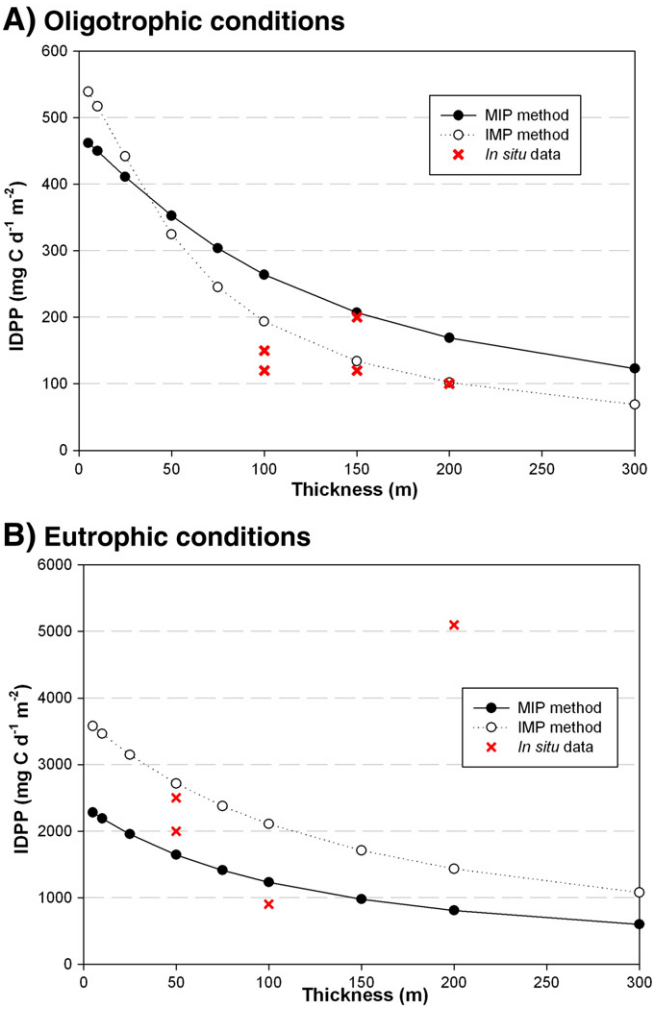

Fig. 3. IDPP values versus thickness of the layer for "oligotrophic" (A) and "eutrophic conditions" (B). Both integration methods are plotted: IMP (white circles) and MIP (black circles).

Table 3
Collected data referenced in the text for the "oligotrophic" and "eutrophic conditions". Data are plotted in the Fig. 3 (a,b).

IDPP (mg C m^{-2} d^{-1})	Thickness (m)	Integrated chlorophyll (mg chl m^{-2})	Location and source
"Oligotrophic conditions"			
120–150	100	~20	Gulf of Cadiz. Navarro et al. (2006)
120–200	150	~20	Eastern North Atlantic Subtropical Gyre Province (NASE). Marañón et al. (2003), Teira et al. (2005)
101	200	30	Canary Islands, Basterretxea and Aristegui (2000)
"Eutrophic conditions"			
2000–2500	~30	~90	Upwelling NO of Spain, Lorenzo et al., 2005)
900	100	75	Gulf of Cadiz (Navarro et al., 2006)
5300	200	150	Canary Islands, Basterretxea and Aristegui (2000)

Both approaches showed a similar response to a varying thickness layer, increasing IDPP with thinner single-layer (Fig. 3a,b). MIP approximation presented a slightly more linear response to varying thickness than IMP method, this behavior was particularly found with "oligotrophic conditions" (Fig. 3a,b). However, average absolute values obtained with IMP are closer to the available data (Fig. 3a,b). Comparing *in situ* data with this 0D experiments was not simple, as it was not possible to collect all the controlling factors values for primary production (PAR, photoperiod or biomass) in the reported bibliography. We have chosen standard values trying to represent the high variability in the data and aiming to use the simulations and data for the decision of the best integration method. With "oligotrophic conditions", computed IMP values (193 mg C m^{-2} d^{-1}, thickness = 100 m; 133 mg C m^{-2} d^{-1}, thickness = 150 m) were lower and more similar to *in situ* data than MIP (Fig. 3a). Measured IDPP in close oligotrophic areas were collected in Table 3 and plotted in Fig. 3a. Furthermore with "eutrophic conditions", IMP values are higher and closer to the available data than MIP approach (Fig. 3b). IDPP in near eutrophic areas were collected in Table 3 and plotted in Fig. 3b. Therefore, we could say that MIP tends to underestimate IDPP with eutrophic and overestimate IDPP with oligotrophic conditions.

Comparing observed and simulated primary production rates is not straight-forward (e.g. Vichi and Masina, 2009). A source of ambiguity of C^{14} uptake method is whether this incubation method is a measure of gross primary production, net primary production or some value in between (Marra, 2009). A recent work showed that C^{14} uptake method tends to underestimate the net primary production, especially in the case of nutrient-stressed cells (Robinson et al., 2009). Consequently, real *in situ* estimates of primary production are likely to be higher than reported in these former works.

Table 4
Forcing factors and boundary conditions designed as sinusoidal functions. Maxima, minima and the respective season are shown.

Variable	Maximum value	Minimum value
Temperature (°C)	23 (summer)	17 (winter)
Chlorophyll concentration (mg m^{-3})	0.3 *	-
Phytoplankton biomass * (mg C m^{-3}) / integrated (mg C m^{-2})	9/2100	-
Nitrate (μM)	1.1 (winter)	0.1 (summer)
Phosphate (μM)	0.25 (winter)	-
Silicate (μM)	8 (winter)	0.1 (summer)
Ammonium (μM)	0.1 (winter)	0.001(summer)

* Phytoplankton biomass, chlorophyll and phosphate concentration in the boundary condition were constant along the year.

Table 5
Description of the collected data of the Atlantic Inflow from previous surveys, aiming to describe the phytoplanktonic seasonal cycle in these waters.

Month	# Profiles (depths)	Research vessel	Survey (year)
February	2 (5)	B/O Cornide de Saavedra	1998
May	4 (6)	BIO Hespérides	2001
June	2(7)	B/O Cornide de Saavedra	1997
September	4(5)	BOA Thalassas,	1997
		B/O Sarmiento de Gamboa	2008
October	2(5)	B/O Sarmiento de Gamboa	2008
November	2(4)	B/O Mytilus	2004

For all of the above reasons, IMP approximation was the chosen method for the integration of primary production in a single-layer and was implemented in the coupled model.

2.3. Design of boundary conditions and forcing factors of the biological model

Boundary conditions are designed to simulate phytoplankton features and seasonal cycle of the Gulf of Cadiz (oligotrophic open-waters), including primary production. Forcing factors and values of variables in boundary conditions are obtained from different sources. PAR was simulated following the standard astronomical equations for photoperiod and maximum daily irradiance from Brock (1981) and the cloud-cover model from Smith and Dobson (1984); using a constant value of 4 oktas following Macías et al. (2007). SST was obtained from satellite (Navarro and Ruiz, 2006). SST and nutrients were simulated as sinusoidal functions based on the available data; season presenting maxima and minima values are shown in Table 4 (Navarro et al., 2006).

In order to set phytoplanktonic features in the boundary conditions, several previous data from Gulf of Cádiz and not modified AI were collected (Table 5 and Fig. 4). These data series were used to fix a constant concentration of chlorophyll and phytoplankton biomass in the boundary conditions (0.3 mg m^{-3} and 9 mg C m^{-3}) (Table 4 and Fig. 5). The ratio between C and chlorophyll used to convert chl data to phytoplankton carbon is derived from Taylor et al. (1997). In the prescribed boundary conditions, the constant chlorophyll and C concentrations derived from bulk observations are equally distributed between the different phytoplankton groups (diatoms, nanoflagellates and picophytoplankton).

3. Results

3.1. Physical variables

The salinity of the surface layer (representing the AI) was used as a proxy for interfacial mixing; in Fig. 5 (a,d), model output was compared to the *in situ* data described in Section 2.1.1. During the first sampled period, the model reproduced the main salinity patterns including two conspicuous peaks (Fig. 5a). *In situ* salinity showed two peaks (36.91 and 36.82) with 6 h of separation (Fig. 5a). Simulated salinity showed also two peaks (36.92) with a semidiurnal frequency (period of 12 h). Minima values from model and measured data matched (36.60–36.63) (Fig. 5a). During the second period of sampling, a central main

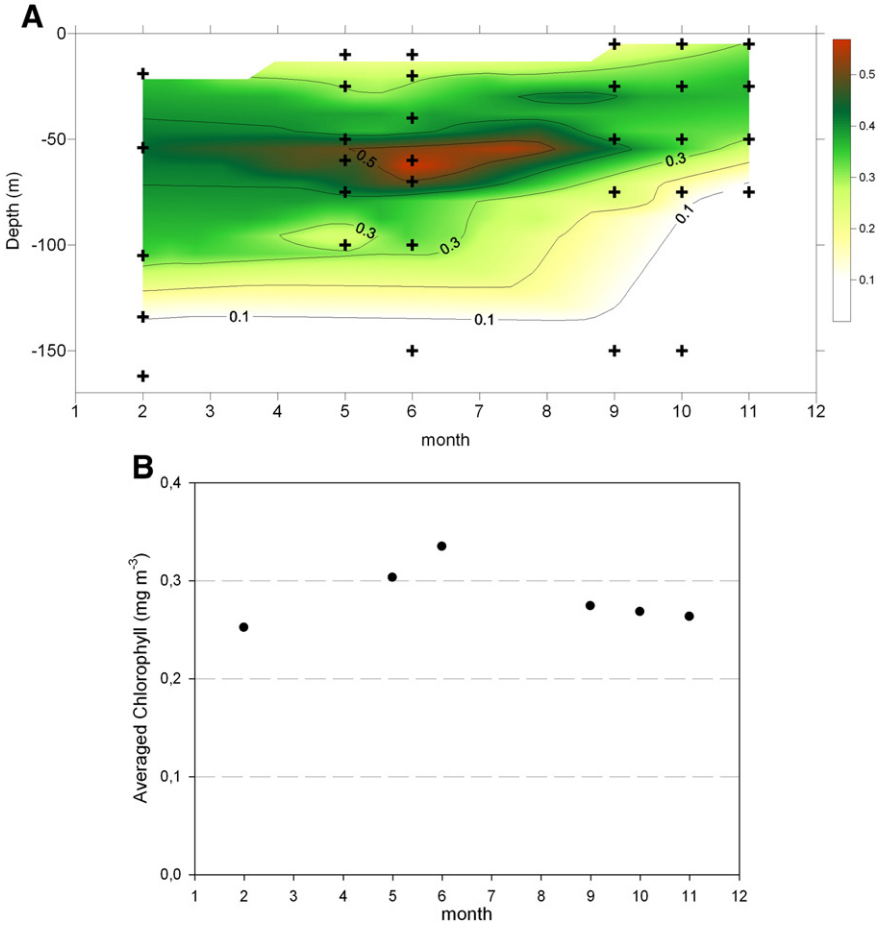

Fig. 4. Reconstructed chlorophyll annual series collected from previous surveys (Table 5). A — Vertical distribution of the chlorophyll concentration (mg m^{-3}) along the year. B — Seasonal cycle of averaged chlorophyll concentration (mg m^{-3}) from collected data.

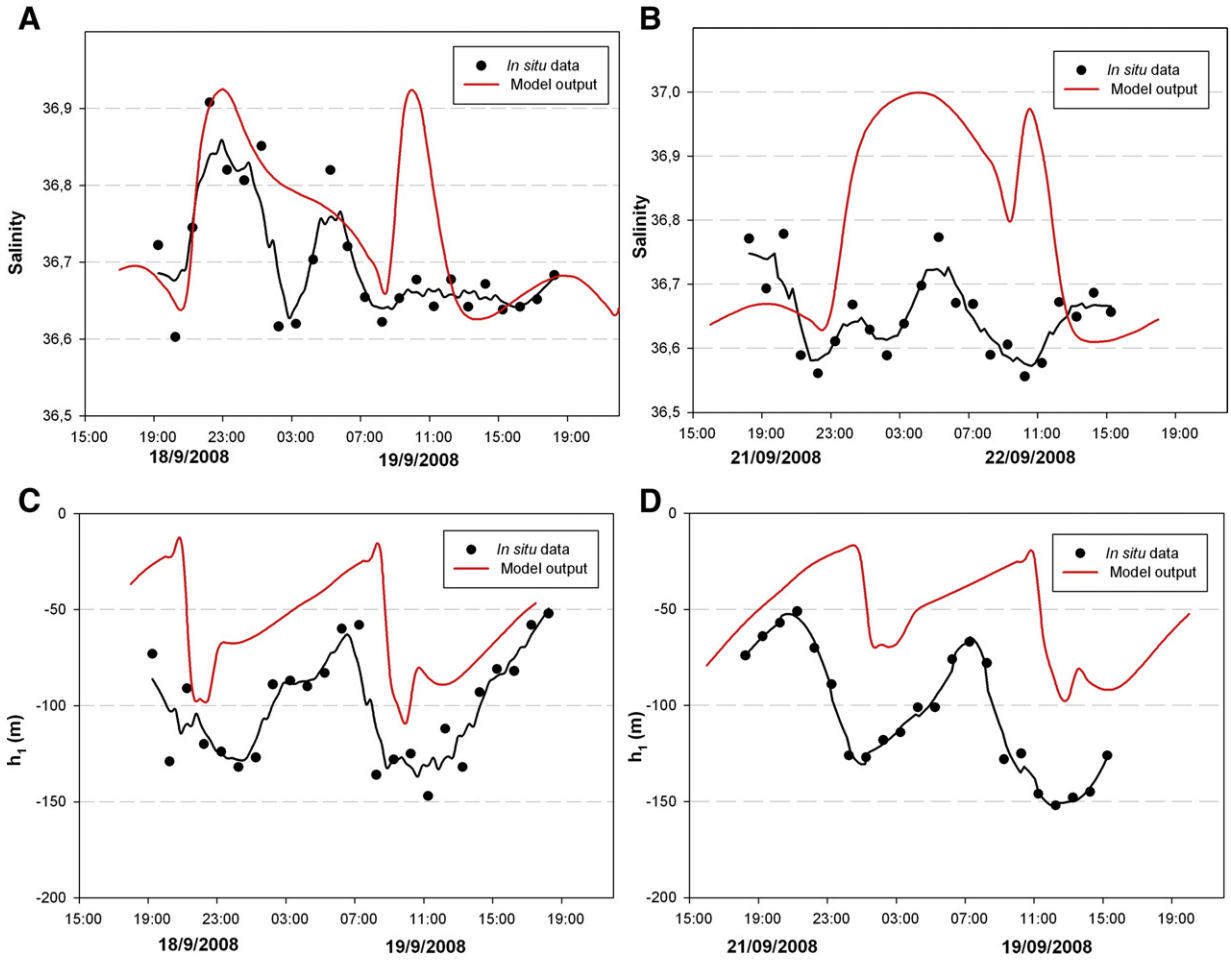

Fig. 5. Model output (red lines) versus *in situ* data from station A (Fig. 1): salinity (A, B); h_1 (AMI or thickness of the layer) (C,D).

peak was found almost reaching 36.78 from measured salinity and 36.99 from simulated one (Fig. 5b). Two minima were found (36.56 and 36.61 respectively) with 12 h of separation (Fig. 3b). This last set of observations was collected during special subinertial forcing conditions. Westward currents, the main forcing agent for the internal wave's generation at Camarinal Sill, were inhibited by an enhanced eastward flow responding to atmospheric forcing over the Western Mediterranean. Thus large amplitude internal wave's generation and the associated vertical mixing processes were not favored (Vázquez et al., 2008). Details concerning these inhibition phenomena are widely explained in Ramírez-Romero et al. (2014).

Salinity as a tracer of interfacial mixing presented two mixing events per day (Fig. 5a,b), this semidiurnal behavior indicates the tidally-related periodicity of the phenomenon (Macías et al., 2007). Peaks correspond to the increased shear that takes place during flood tide (García-Lafuente et al., 2000, 2002; Izquierdo et al., 2001). Spatially, mixing processes dominate around Camarinal Sill, with a secondary area around Tarifa Narrows (Fig. 6) in good agreement with some previous works (e.g. Macías et al., 2007; Sannino et al., 2007).

The physical model reproduced the general patterns of the surface layer thickness h_1, which is equivalent to the AMI depth in the data. *In situ* data oscillated from −50 to −150 m and the simulated h_1 moved from −25 to −100 m (Fig. 5b and d). The model in general underestimates the thickness but the relative change during the observed period was correctly simulated (Fig. 2 d).

These results described above confirm an acceptable behavior of the model that allowed us to investigate the response at the longer seasonal scale (Fig. 7). To accomplish this, one whole year simulation was performed. Along the simulated year and in addition to the semidiurnal cycle, salinity at the easternmost nodes (Eastern Strait) showed a fortnightly variation (Fig. 7a). Spring tides showed the largest salinity ranges, from 36.65 to 37.11. Highest salinity along the year was found during spring equinoctial tides (37.11) (March) and autumn (September) (Fig. 7a)

Annual-averaged h_1 are plotted together with the corresponding standard deviation and the bathymetry of the model (Fig. 7b). The thickness of the upper layer was about 200 m westward of Camarinal Sill, decreasing eastward and reaching 40 m in the easternmost nodes of the domain. The highest standard deviations were found above Camarinal Sill and nearby grid points (Fig. 6b). Therefore, the model was able to reproduce the reduction of the thickness (h_1) of the surface layer from west to east (Fig. 7b) and the large oscillation of this layer over the main Sill of the Strait (e.g. Bray et al., 1990; Ramírez-Romero et al., 2012)

3.2. Biogeochemical variables

Biogeochemical variables are shown in both sides of Camarinal Sill, aiming to observe the westward Atlantic features and the modifications after AI crosses the Strait. Biogeochemical results are shown for Western Strait (WS) (30 averaged nodes) (Figs. 2 and 6b), representing features of the open-waters of the Gulf of Cadiz forming the AI and for the easternmost nodes (Eastern Strait, 30 averaged nodes)(ES) (Figs. 2 and 7 b).

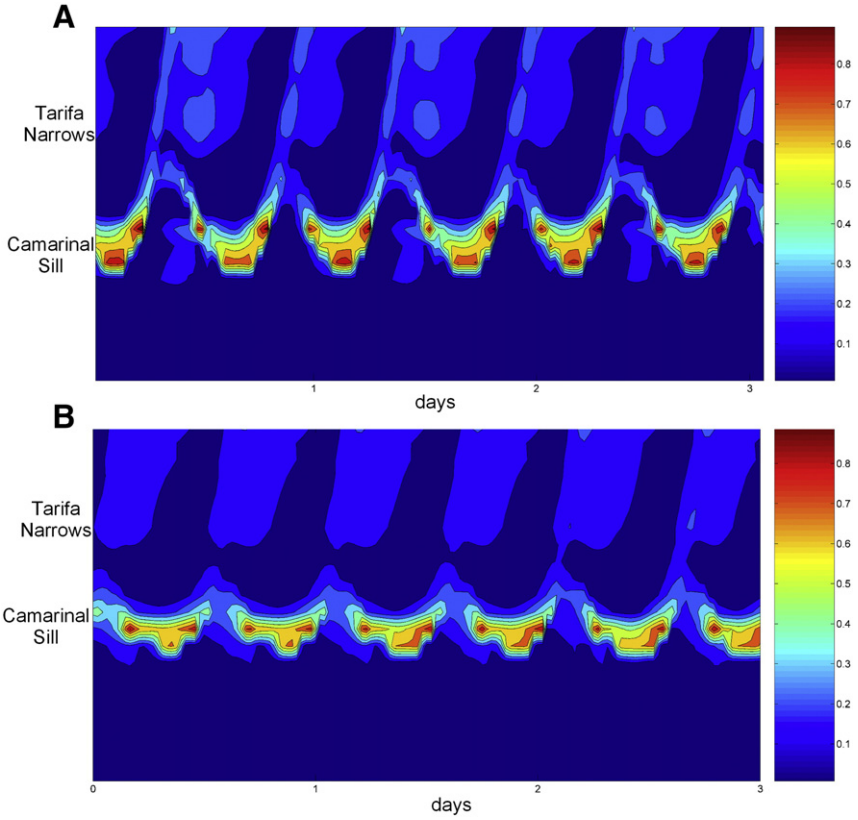

Fig. 6. Spatio-temporal distribution of the index of mixing ($F_1{}^2$, Eq. (2)) during three days of simulations for spring tides (A) and neap tides (B).

Nitrate concentration at WS followed a sinusoidal curve as a consequence of the designed boundary conditions (Section 2.3), oscillating from winter (1 μM) to summer (0.1 μM) (Fig. 8a). During spring tides some nitrate peaks were found (1 μM); mixed waters from Camarinal Sill could reach WS (Fig. 8 a) when currents revert westward. The annual nitrate series at ES showed higher values and a less marked seasonal cycle than at WS (Fig. 8a). Nevertheless, nitrate followed the same spring/neap tides modulation than salinity (Fig. 7a), as an example of this, during spring tides the concentration could reach 2.5 μM (summer) or even 3.5 μM (during the rest of the year) (Fig. 8a).

Phytoplankton biomass, as the sum of the three phytoplankton functional group concentrations, presented a seasonal cycle (Fig. 8b) at the WS: maximum value (11 mg C m^{-3}) was found in spring (from April to June): minimum value (8 mg C m^{-3}) in summer (July–August) and finally a secondary maximum (slightly higher than 10 mg C m^{-3}) was found in autumn (September). In the ES, biomass followed the same seasonal cycle trends than in the WS (Fig. 7b). However, both, first and second maxima reached higher values, 15 and 13 mg C m^{-3} respectively. Minimum values (summer) were in the same range than at WS (8 mg m^{-3}).

Unfortunately, there are no previous works showing the annual cycle of phytoplankton biomass in the open waters of the Gulf or in the Strait; in order to compare with the results in WS/ES from the model. The scattered biomass values from previous works are collected in Table 6. *In situ* data are in the range or slightly higher than those showed by the model (Fig. 8a and Table 6). Therefore, the annual cycle depicted by our model could be regarded as a reasonable approach to seasonal plankton dynamics in the region.

Primary production, in terms of IDPP, followed the same seasonal trends described for the phytoplankton biomass (Fig. 7c). In the WS maximum value occurred during spring (almost 1200 mg C m^{-2} day^{-1}), and minimum during summer (400 mg C m^{-2} day^{-1}). There was also a secondary maximum in autumn (900 mg C m^{-2} day^{-1}). In addition, IDPP at ES presented the same cycle (Fig. 7c); however most of the year absolute values were slightly lower than production at WS. Only during some period (from April to September) and during some peaks, IDPP at ES could be higher than at WS reaching 1500 mg C m^{-2} day^{-1}. Chlorophyll concentration in both sides of the Strait approximately followed the seasonal trend of the biomass, presenting maxima during spring/autumn (slightly higher than 0.3 mg m^{-3}) and minima during summer (0.25 mg m^{-3})(Fig. 7b, d). Former reported values of IDPP in the Strait and in the AI are collected in Table 6. Measured values are lower than those simulated in this work (Table 6 and Fig. 8c). Surprisingly these low measured values matched with high nutrients concentrations (nitrate ~3 μM) and chlorophyll maxima (0.4 mg m^{-3}) close to surface (Macías et al., 2009). Our simulations also fall in this range of chlorophyll and nitrate (Fig. 7a,d) but simulated IDPP are considerably higher (Fig. 8c).

The relative (%) biomass of phytoplankton for each simulated functional group (diatoms, nanoflagellates and picophytoplankton) also presented a seasonal succession along the year (Fig. 9a). Biomass is more or less equally distributed among the groups during winter, particularly in the WS. However, during the spring and autumn biomass maxima (Fig. 8b) nanoflagellates dominated (45% and 40% respectively) (Fig. 9 a). Furthermore, during the late summer minimum of biomass (Fig. 8b), picophytoplankton was the predominant group (almost 50%, Fig. 9a). At the eastern boundary (ES), the percentage of nanoflagellates was higher than at WS (Fig. 9b), 40% along most of the year and reaching 50 and 45% in the first and second peaks, respectively. During summer and at the ES, picophytoplankton reached almost 60% of the phytoplankton biomass (Fig. 9b). Coinciding with these simulated functional groups, nanoflagellates and picophytoplankton (Fig. 9) groups have been described as the most representative groups for open Atlantic waters in the Gulf and in the AJ at the closest Alboran Sea (Table 6) (Echevarría et al., 2009; Reul et al., 2005).

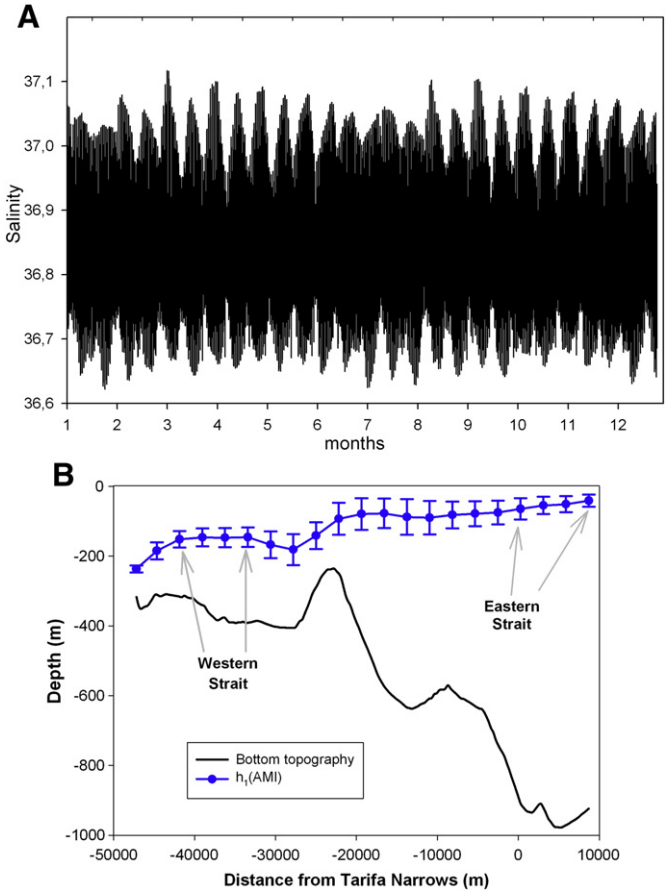

Fig. 7. A – Time series along the year of salinity in the easternmost nodes or sections of the domain (Eastern Strait). B – Bathymetry of the domain (black line), average position of the AMI (h_1) (blue line) and standard deviation. Eastern and Western Strait sections are marked.

4. Discussion

4.1. Physical results

In spite of the apparently simplicity of the physical model, it reproduces satisfactorily the main physical features of the main channel of the Strait (Fig. 2). Features of the model include tidal forcing, two layers and it also takes into account the width and depth of the Strait (see Section 2.1); thus it could be considered as a "1.5D" model. The model could solve very high resolution crucial processes for the biological coupling as the decrease of the surface layer thickness and mixing dynamics (see Section 3.1). Furthermore, the relative simplicity of the model allowed a non excessively expensive computational demand of the simulations facilitating the coupling with a complex biogeochemical model as Biogeochemical Fluxes Model. The annual simulations solving high resolution tidal scales allows to report seasonal cycles of biogeochemical features in the Strait, as one of the main findings of this work. This is, so far, the first coupled model that solves tidal forcing at the Strait using a fully-coupled way, a finite-volume scheme and a Plankton Functional Type model.

At annual scales, salinity in the eastern boundary showed a modulation due to the spring/neap tidal cycle (fortnightly variation) (Fig. 7a). Mixing was less intense during neap tides but still significant (Fig. 6b and 7 a). This phenomenon is attributable to the parameterization of mixing processes (Eqs. (2) and (5)) which is mainly proportional to the shear between layers. As it was shown by Bruno et al. (2010), at subinertial scales non linear interactions among tidal components of the flow minimize the differences of maximum shear between neap and spring tides. This process is likely to contribute to a more regular interfacial mixing than would be expected if only semidiurnal tide dynamics were considered. This fact has consequences on the biological features as it will be explained below.

4.2. Biogeochemical variables

4.2.1. Biogeochemical features in the original Atlantic Inflow

The boundary conditions presented in Section 2.3 were set up to simulate the pelagic dynamics of open-ocean waters of the Gulf of Cadiz using all the data available from previous surveys (Fig. 4). This is the first work reporting the seasonal cycle in biomass and IDPP in the Strait of Gibraltar. Main features included a maximum in spring, a minimum during summer and a secondary maximum during autumn (WS; Fig. 7b,c). Seasonal cycle here was forced by the annual irradiance curve (maximum value in summer) and nutrients availability (minimum value in summer/deep mixing in winter, Fig. 8a)(Navarro et al., 2006).Therefore, biomass maxima were found then when there is a coincidence of enough nutrients and light to support phytoplankton growing, mainly during spring and autumn (Fig. 7a).

This seasonal cycle is similar to the biogeographical classification proposed by Longhurst (1995) in the "Model 2" bio-province, *mid-latitude nutrient limited spring production peak* or even in the Model 8 bio-province, *canonical nutrient-limited spring bloom of temperate waters*. The expected mechanism for this original pattern is the "Gran effect" or the "Critical-depth hypothesis" (Sverdrup, 1953). However, the simulated h_1 is only dependent on tidal forcing, thus concepts as "mixed layer" or "critical depth" cannot be used in this single-layer model. In spite of this simplified seasonal forcing (Fig. 8) it collects the main features of the seasonal cycles in temperate waters. These results will be used as a base line to assess the role of the physical processes occurring in the Strait and how the original features of the Atlantic Inflow are modified.

4.2.2. Effect of the Strait of Gibraltar on biogeochemical features

Coastal-channel interactions cannot be taken into account in a 1D two-layer model. Consequently, the characteristic advection of chlorophyll patches from coastal areas (Vázquez et al., 2009) cannot be reproduced by the model. We remark that these patches were only detected during 2–3 h in each tidal cycle (12 h) and mostly during spring tides (Macías et al., 2006; Ramírez-Romero et al., 2014). Furthermore during spring tides, an important amount of mixed waters did not traveled eastward concurrent with the chlorophyll patches (Ramírez-Romero et al., 2014). Therefore, this coupled model covered a wide part of the Atlantic Inflow and these results may be considered as the background processes in the Atlantic Jet, excluding the intermittent presence of coastal patches.

Despite the prescribed along-year constant boundary conditions (Table 4), there is a biomass increase in the Atlantic Inflow at Eastern Strait right after the Strait, especially notable during spring and autumn (Fig. 8b). Regarding primary production, simulated IDPP in the eastern side of the Strait was in the same range or even higher than in the western side (Fig. 8c). However, the thickness of surface layer is thinner eastward of the sill than westward (Fig. 7b). Therefore per unit of volume, values of primary production in the eastern side were 3-times higher than westward of the sill (data not shown).The model explains this as a combination of mixing processes around Camarinal Sill (Fig. 6) that provide high nutrient concentrations (Fig. 8a) in concomitance with a thinner surface layer in the eastern side of the Strait (Fig. 7b). This mechanism resembles the "Gran effect" (Gómez et al., 2000), as high nutrients and phytoplankton are found in a shoaling well-illuminated layer. However, this mechanism presents a tidal-related periodicity, mostly semidiurnal (Fig. 5a,b and 7 a). As shown before (Section 3.2) mixing also occurs during neap tides (Fig. 6b and 7 a), allowing a nutrient input and active growing also during these periods.

On the other hand, intense mixing may lead to important biomass losses from the surface layer (strong dilution). Thus, at short temporal

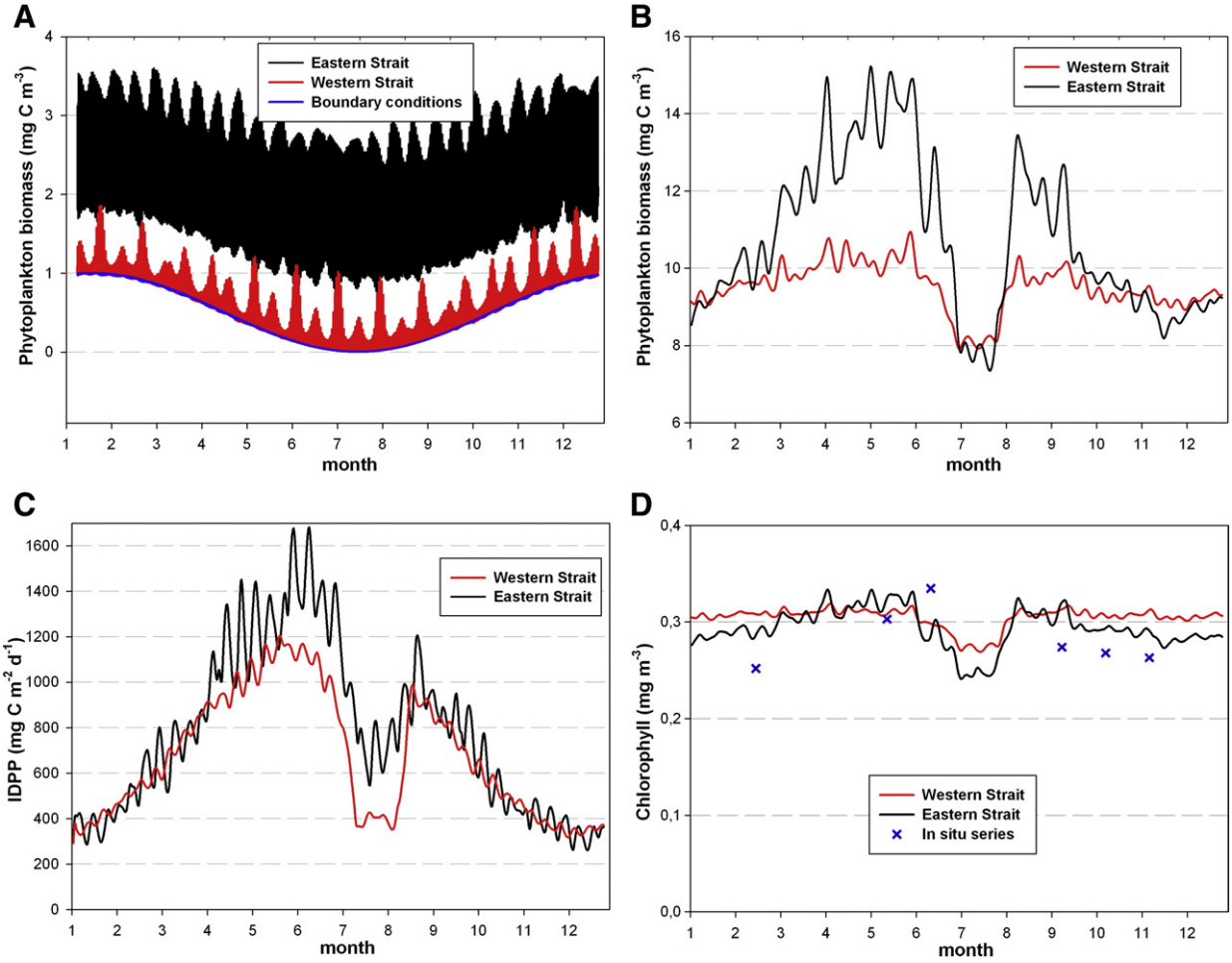

Fig. 8. A – Time series along the year of nitrate concentration in the Western Strait section (WS) (red line) and in the Eastern Strait section (ES) (black line). B – Time series along the year of smoothed phytoplankton biomass in the WS (red line) and in the ES (black line). C – Time series along the year of IDPP in the WS (red line) and in the ES (black line). D – Time series along the year of chlorophyll concentration in the WS (red line) and in the ES (black line).

scale in the Strait there are two opposite processes regarding phytoplankton biomass: growth (primary production) versus mixing. Macías et al. (2007) found a decrease of phytoplankton biomass along the Strait due to intense mixing concentrated around Tarifa Narrows. Coinciding with this fact during summer and winter, biomass increase in the eastern side could not be appreciated (Fig. 8b). This fact could indicate that this fast response and increase of the phytoplankton biomass could depend on physiological state of the cells, simulated by the internal ratios of the BFM. With unfavorable conditions, light or nutrients during winter and summer respectively, simulated populations need more time to adapt internal ratios and to present an effective increase of the biomass. This response could be simulated due to the use of flexible component ratios of the equations of the BFM (Vichi et al., 2007b).

Regarding large differences found between simulated and measured IDPP, Macías et al. (2009) suggested that photoinhibition could cause unexpected low values in the observations (Table 6). Given enough time, the Strait dynamics could raise a deep chlorophyll maximum from 100 m to the surface in approximately one day (Macías et al., 2007, 2008). Specifically, Bartual et al. (2011) found that this raising of the maximum could occur in ~20 min in the vicinity of the sill. Also, this maximum is under high turbulent levels and vertical velocities (Wesson and Gregg, 1994); favoring the exposition of the phytoplankton to harmful light levels. BFM does not include photoinhibition in its formulation (Vichi et al., 2007b), thus this mechanism could not be appreciated in our results. In addition, Morán and Estrada (2001) reported higher IDPP (330 mg C m^{-2} d^{-1}) values westward within the Alboran Sea (Atlantic Jet and West Alboran Gyre), and Arin et al. (2002) reported an active growth of phytoplankton in that same station. An explanation for this could be that after passing through the Strait,

Table 6
Description of the previous collected data of the Atlantic Inflow/Strait of Gibraltar area from previous surveys, aiming to describe the phytoplanktonic seasonal cycle in these waters and compare to the output of the model at Western Strait (WS) or Eastern Strait (ES).

Place	Value	Source
"Phytoplankton biomass (mg C m^{-3})"		
Gulf of Cádiz (WS)	0–15 (cells Ø < 13 μm)	Reul et al. (2006)
Gulf of Cádiz (WS)	5 (picophytoplankton)	Echevarría et al. (2009)
Open Atlantic Waters (Subtropical Gyre) (WS)	5–10	Marañón et al. (2000)
Strait of Gibraltar (ES)	18–50	Reul et al. (2002, 2008)
Atlantic Jet (Alboran Sea) (ES)	40–50 (24 summer)	Reul et al. (2005)
"IDPP-Integrated Daily Primary Production (mg C d^{-1} m^{-2})"		
Gulf of Cádiz (WS)	120–150	Navarro et al. (2006)
Strait of Gibraltar (ES)	14–66	Macías et al. (2009)
Strait of Gibraltar (ES)	82 ± 54	Bartual et al. (2011)
"% Functional groups"		
Gulf of Cádiz (WS)	50 (picophytoplankton)	Echevarría et al. (2009)
Atlantic Jet (Alboran Sea) (ES)	40–70 nanoflagellates (50% picophytoplankton in summer)	Reul et al. (2005)

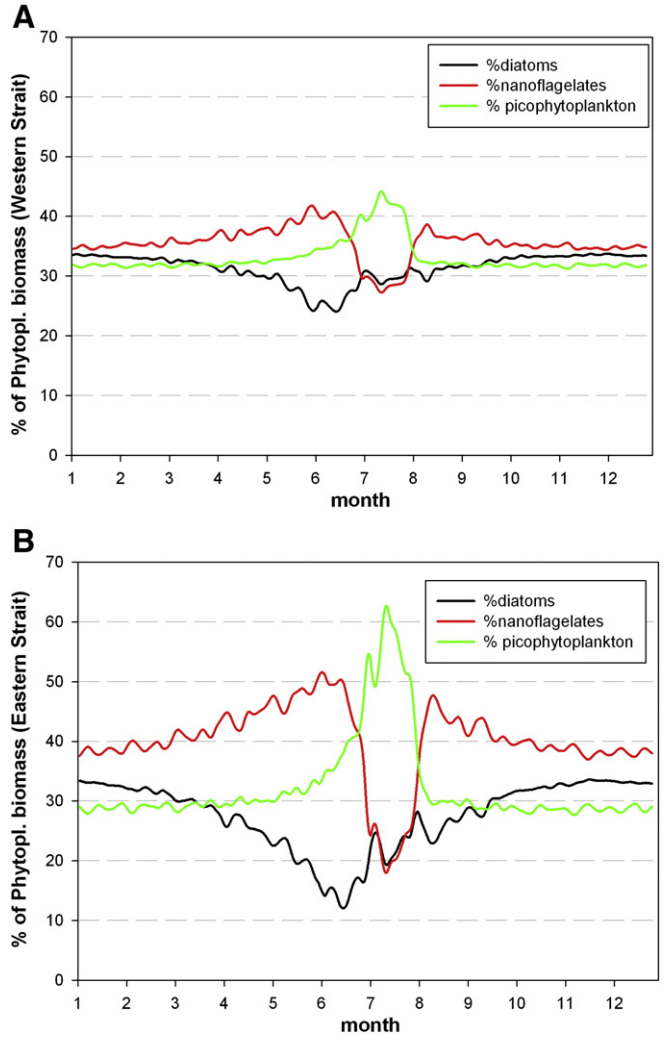

Fig. 9. A – Relative abundance (% of biomass) of phytoplankton groups in the Western Strait. B – Relative abundance (% of biomass) of phytoplankton groups in the Eastern Strait.

phytoplankton communities in the Atlantic Jet need a relative long time to become acclimated to the new light conditions.

In general terms, the relative importance of picophytoplankton decreases from the Gulf of Cádiz towards Alborán Sea, because of the upwelling processes in this area (Echevarría et al., 2009). However this pattern is not applicable in the Atlantic Jet influence area and in the West Alboran Gyre (Table 6) (Arin et al., 2002; Reul et al., 2005). This was also the case in our results (Fig. 9 b). Nevertheless, the intense physical processes in the Strait force the waters to have a short residence time in the eastern part of the domain, around 22 h, similar to the results of Macías et al. (2007). This time span did not allow observing a posterior evolution of the phytoplankton immersed in high nutrients and high light levels. At this short scale only the fast responding groups with high intrinsic growth rates could be observed to have a response (picophytoplankton or nanoflagellates) (Fig. 9b). A fast response of nanoflagellates to the biogeochemical changes occurring in the Strait was also showed by Reul et al. (2008). At longer scales, the phytoplankton biomass would tend to be larger in this favorable conditions and the group succession in the Atlantic Jet could be different. In these long scales, microzooplankton should be included, as picophytoplankton is continuously under grazing control (e.g. Quevedo and Anadón, 2001; Taylor et al., 1993).

To summarize, we collected the relevant results showed above in a "Longhurst diagram" (Fig. 10), proposing this seasonal cycle for the Strait of Gibraltar region (Eastern Strait, Fig. 1). In this diagram we replaced the originally mixed-layer depth by an equivalent AMI depth for this case (Fig. 10b). There was a tidal signal (mostly semidiurnal) superimposed over this cycle, not taken into account in this figure for an overall visualization of the results. We suggest these results for inclusion as boundary conditions or input for biological models of the Mediterranean Sea. This would provide an improved dynamical modulation to constant boundary conditions that is currently used in models (e.g. Lazzari et al., 2012).

4.3. Influence of AI on the trophic state of the Mediterranean

The Alboran Sea has been described as the most productive area in the Mediterranean Sea (Siokou-Frangou et al., 2010). In this area, Lazzari et al. (2012) estimated an integrated production of 274 ± 11 g C m^{-2} $year^{-1}$, defining this area as mesotrophic (production between 100 and 300 g C m^{-2} $year^{-1}$), while the eastern Mediterranean is typically oligotrophic. In this work, the Atlantic Inflow in the easternmost side of the Strait presented an integrated production of 105 g C m^{-2} $year^{-1}$, which is at the lower limit of this range. Nevertheless the Atlantic Inflow containing constantly higher nutrient levels and actively growing phytoplankton could have an effect of fertilization and biomass increase in the upper layer of the NW Alboran Sea. Coastal upwelling has been described as a crucial process to enhance the primary production in this area (e.g. Macías et al., 2009). However, the effect of the Atlantic Inflow should not be disregarded (Oguz et al., 2013). Using this crude approximation of the Atlantic Inflow without taking into account the role of NACW, Atlantic Inflow could supply about 275 tons m^{-1} $year^{-1}$ (4.43 megamol m^{-1} $year^{-1}$) of nitrate to the surface Alboran Sea. Sarhan et al. (2000) reported 13.9 tons m^{-1} $year^{-1}$ (0.22 megamol m^{-1} $year^{-1}$) of nitrate, summing different modes of upwelling in Alboran Sea (northwestern coast). It should be said that these values are per linear meter parallel to the coast, being the Strait section about 20 km at the easternmost boundary in our domain and the coastal upwelling extending ~50 km. Performing the calculations, it could be computed that these phenomena mean 4.95 and 0.70 megatons nitrate $year^{-1}$ (79.83 and 11.79 gigamol $year^{-1}$) respectively, being the Strait's supply considerably higher than that of the coastal upwelling. This value is in agreement with observation-based estimates. Huertas et al. (2012) reported that the Atlantic layer might input about 4.69 megatons $year^{-1}$ of nitrate (75.64 gigamol $year^{-1}$). Thus, during inactive periods of this coastal upwelling, the relevance of the Strait raises, as it plays a role of quasi-constant fertilization of the Alboran Sea.

Regarding phytoplankton biomass transport, our estimates show that AI may supply to the Alboran Sea about 1211 ± 233 tons C d^{-1} (44 ktons C $year^{-1}$); with a summer minimum of 750 tons C d^{-1} and spring maximum of 1700 tons C d^{-1}. There is only one reported value for this supply. Reul et al. (2002) from *in situ* data for a single-day measurement, reported an autotrophic biomass of ~2500 tons C d^{-1}. In addition it is worth saying this phytoplankton biomass is transported in favorable conditions for growth, immersed in high nutrients concentration and high light levels.

Aiming to improve our understanding of biological processes in the Strait, more complex and extended models should be developed. In the physical part, this model should include 2D or 3D dynamics in order to analyze coastal-channel interactions. Biological model should include photoinhibition processes aiming to investigate the unexpectedly low primary production values in the Strait. Also, model domain should be extended towards the Alboran Sea for observing the evolution of the plankton communities under new conditions after passing through the Strait, including zooplankton dynamics. All this processes should be backed up with corresponding observations.

5. Conclusions

This work presents the effects on phytoplankton of the processes occurring in the Strait of Gibraltar that modify the biogeochemical

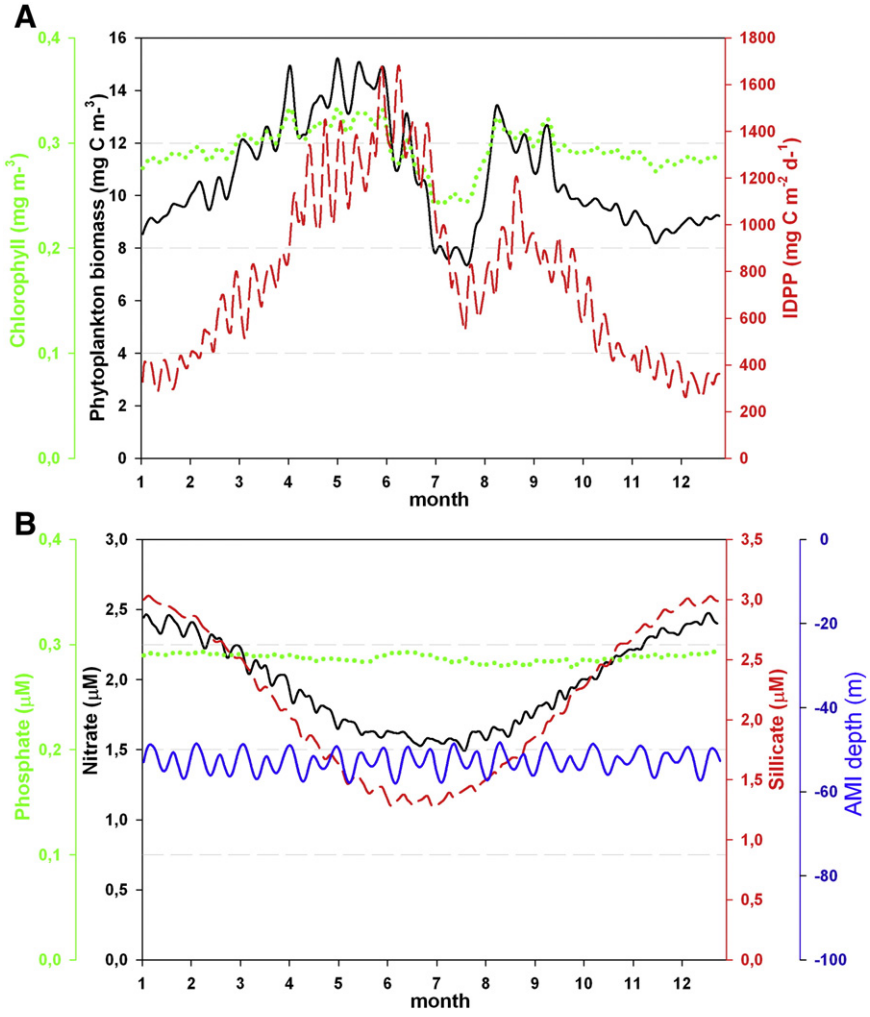

Fig. 10. Longhurst diagram for the Strait of Gibraltar (Eastern Strait). A: Black line represents Phytoplankton biomass (mg C m^{-3}). Green dotted line represents Chlorophyll concentration (mg m^{-3}). Red broken line represents IDPP (mg C m^{-2} d^{-1}). B: Black line represents Nitrate concentration (µM). Green dotted line represents Phosphate concentration (µM). Red broken line represents Silicate concentration (µM). Blue line represents AMI depth (m), the equivalent thickness of the surface layer.

features of the Atlantic Inflow. This model is capable to resolve crucial high-resolution processes such as tidal forcing while at the same time maintaining a very efficient performance that allows to study biogeochemical patterns at the longer seasonal scales. The model shows the emergence of the phytoplankton seasonal cycle in the Atlantic Inflow coming from the Gulf of Cádiz. Main characteristics are biomass and primary production maxima during summer and autumn, when nanoflagellates are the most representative phytoplankton group. Minima of biomass and production in the Atlantic Inflow are found during the summer season dominated by picophytoplankton. The physical processes in the Strait induce a relatively constant nutrient supply and a thinner surface layer (raising the available light for phytoplankton). These phenomena trigger primary production and raise phytoplankton biomass, especially during spring and autumn. These processes also modified the seasonal succession in the Atlantic Inflow at shorter scales, intensifying the dominance of nanoflagellates (spring and autumn) and picophytoplankton (summer). The presence of these processes may thus imply a quasi-permanent fertilization of the surface Alboran waters through a relevant supply of nitrate and well-acclimated phytoplankton.

Acknowledgements

This work was supported by the Spanish National Research Plan; projects: CTM2005-08142C03-01 and CTM2008-06124. E.R-R was supported by a grant from the FPU fellowship program. D.M. was supported by a JaeDOC contract (#X0SC000087) of the Spanish Council for Scientific Research (CSIC) and by a Cat30 grant holder position of the Joint Research Center of the European Commission. We also thank Dr. Gabriel Navarro for providing data from previous works of the Gulf of Cádiz. M.V. acknowledges the support of the PERSEUS project funded by the EU under FP7 Theme "Oceans of Tomorrow" OCEAN.2011-3 (No. 287600). E.R-R. gratefully acknowledges the support of the European Commission (OCEAN-CERTAIN, FP7-ENV-2013-6.1-1; no: 603773). We thank the anonymous reviewers for their constructive comments. This is the contribution no. 67 from the CEIMAR Journal Series.

References

Arin, L., Morán, X., Estrada, M., 2002. Phytoplankton size distribution and growth rates in the Alboran Sea (SW Mediterranean): short term variability related to mesoscale hydrodynamics. J. Plankton Res. 24, 1019–1033.

Bartual, A., Macías, D., Gutierrez-Rodriguez, A., Garcia, C., Echevarría, F., 2011. Transient pulses of primary production generated by undulatory processes in the western sector of the Strait of Gibraltar. J. Mar. Syst. 87, 25–36.

Basterretxea, G., Aristegui, J., 2000. Mesoscale variability in phytoplankton biomass distribution and photosynthetic parameters in the Canary-NW African coastal transition zone. Mar. Ecol. Prog. Ser. 197, 27–40.

Bray, N., Winant, C., Kinder, T., Candela, J., 1990. Generation and kinematics of the internal tide in the Strait of Gibraltar. In: Pratt, L. (Ed.), The physical oceanography of sea straits. Kluwer, Boston.

Brock, T., 1981. Calculating solar radiation for ecological studies. Ecol. Model. 14, 1–19.

Bruno, M., Alonso, J.J., Cózar, A., Vidal, J., Ruiz-Cañavate, A., Echevarría, F., Ruiz, J., 2002. The boiling-water phenomena at Camarinal Sill, the strait of Gibraltar. Deep-Sea Res. II 49, 4097–4113.
Bruno, M., Macías, J., González-Vida, J.M., Vázquez, A., 2010. Analyzing the tidal-related origin of subinertial flows through the Strait of Gibraltar. J. Geophys. Res. 115, C12075.
Castro, M.J., García-Rodríguez, J.A., González-Vida, J.M., Macías, J., Parés, C., Vázquez-Cendón, M.E., 2004a. Numerical simulation of two-layer shallow water flows through channels with irregular geometry. J. Comput. Phys. 195, 202–235.
Castro, M.J., Macías, J., Parés, C., García-Rodríguez, J.A., Vázquez-Cendón, E., 2004b. A two-layer finite volume model for flows through channels with irregular geometry: Computation of maximal exchange solutions. Commun. Nonlinear Sci. Numer. Simul. 9, 241–249.
Castro, M.J., Gonzalez-Vida, J.M., Macias, J., Pares, C., 2009. Realistic applications of a tidal 2d two-layer shallow water model to the strait of Gibraltar. In: Simos, T.E., Psihoyios, G., Tsitouras, C. (Eds.), Numerical analysis and applied mathematics. Amer Inst Physics, vols. 1 and 2, pp. 1429–1432.
Criado-Aldeanueva, F., Garcia-Lafuente, J., Vargas, J.M., Del Río, J., Vázquez, Á., Reul, A., Sánchez, A., 2006. Distribution and circulation of water masses in the Gulf of Cadiz from in situ observations. Deep-Sea Res. II 53, 1144–1160.
Cushman-Roisin, B., 1994. Introduction to geophysical fluid dynamics (Chapter 11). Prentice-Hall (320 pp.).
Ebenhoh, W., Baretta-Bekker, J., Baretta, J., 1997. The primary production module in the marine ecosystem model ERSEM II, with emphasis on the light forcing. J. Sea Res. 38, 173–193.
Echevarría, F., Zabala, L., Corzo, A., Navarro, G., Prieto, L., Macias, D., 2009. Spatial distribution of autotrophic picoplankton in relation to physical forcings: the Gulf of Cadiz, Strait of Gibraltar and Alboran Sea case study. J. Plankton Res. 31, 1339–1351.
Evans, G., Parslow, J., 1985. A model of annual plankton cycles. Biol. Oceanogr. 3, 327–347.
Fasham, M.J.R., Ducklow, H., McKelvie, S., 1990. A nitrogen-based model of plankton dynamics in the oceanic mixed layer. J. Mar. Res. 48, 591–639.
Fernández-Nieto, E.D., Narbona-Reina, G., 2008. Extension of WAF Type Methods to Non-Homogeneous Shallow Water Equations with Pollutant. J. Sci. Comput. 36, 193–217.
Franks, P.J.S., Chen, C., 2001. A 3-D prognostic numerical model study of the Georges bank ecosystem. Part II: biological-physical model. Deep-Sea Res. II 48, 457–482.
García-Lafuente, J., Vargas, J., Plaza, F., Sarhan, T., 2000. Tide at the eastern section of the Strait of Gibraltar. J. Geophys. Res. 105, 197–213.
García-Lafuente, J., Delgado, J., Vargas, J., Vargas, M., Plaza, F., Sarhan, T., 2002. Low-frequency variability of the exchanged flows through the Strait of Gibraltar during CANIGO. Deep-Sea Res. II 49, 4051–4067.
Gascard, J., Richez, C., 1985. Water masses and circulation in the western Alboran Sea and in the Straits of Gibraltar. Prog. Oceanogr. 15, 157–216.
Gómez, F., Gonzalez, N., Echevarría, F., García, C.M., 2000. Distribution and fluxes of dissolved nutrients in the strait of Gibraltar and its relationships to microphytoplankton biomass. Estuar. Coast. Shelf Sci. 51, 439–449.
Huertas, I.E., Ríos, A.F., García-Lafuente, J., Navarro, G., Makaoui, A., Sánchez-Román, A., Rodriguez-Galvez, S., Orbi, A., Ruíz, J., Pérez, F.F., 2012. Atlantic forcing of the Mediterranean oligotrophy. Global Biogeochem. Cycles 26, 1–9.
Izquierdo, A., Tejedor, L., Sein, D., Backhaus, J., Brandt, P., Rubino, A., Kagan, B., 2001. Control variability and internal bore evolution in the Strait of Gibraltar: A 2-D two-layer model study. Estuar. Coast. Shelf Sci. 53, 637–651.
Lacombe, H., Richez, C., 1982. The regime of the Strait of Gibraltar. In: Nihoul, N. (Ed.), Hydrodynamics of Semienclosed Seas. Elsevier, New York.
Lazzari, P., Solidoro, C., Ibello, V., Salon, S., Teruzzi, a., Béranger, K., Colella, S., Crise, a., 2012. Seasonal and inter-annual variability of plankton chlorophyll and primary production in the Mediterranean Sea: a modelling approach. Biogeosciences 9, 217–233.
Longhurst, A., 1995. Seasonal cycles of pelagic production and consumption. Prog. Oceanogr. 36, 77–167.
Lorenzo, L.M., Arbones, B., Tilstone, G.H., Figueiras, F.G., 2005. Across-shelf variability of phytoplankton composition, photosynthetic parameters and primary production in the NW Iberian upwelling system. J. Mar. Syst. 54, 157–173.
Macías, D., García, C.M., Echevarría Navas, F., Vázquez-López-Escobar, A., Bruno Mejías, M., 2006. Tidal induced variability of mixing processes on Camarinal Sill (Strait of Gibraltar): A pulsating event. J. Mar. Syst. 60, 177–192.
Macías, D., Martin, a.P., García-Lafuente, J., García, C.M., Yool, a., Bruno, M., Vázquez-Escobar, a., Izquierdo, a., Sein, D.V., Echevarría, F., 2007. Analysis of mixing and biogeochemical effects induced by tides on the Atlantic–Mediterranean flow in the Strait of Gibraltar through a physical–biological coupled model. Prog. Oceanogr. 74, 252–272.
Macías, D., Lubián, L.M., Echevarría, F., Huertas, I.E., García, C.M., 2008. Chlorophyll maxima and water mass interfaces: Tidally induced dynamics in the Strait of Gibraltar. Deep-Sea Res. I 55, 832–846.
Macías, D., Navarro, G., Bartual, A., Echevarría, F., Huertas, I.E., 2009. Primary production in the Strait of Gibraltar: Carbon fixation rates in relation to hydrodynamic and phytoplankton dynamics. Estuar. Coast. Shelf Sci. 83, 197–210.
Malanotte-Rizzoli, P., Artale, V., Borzelli-Eusebi, G.L., Brenner, S., Civitarese, G., Crise, A., Font, J., Gacic, M., Kress, N., Marullo, S., Ozsoy, E., Ribera d'Alcalà, M., Roether, W., Schroeder, K., Sofianos, S., Tanhua, T., Theocharis, A., Alvarez, M., Ashkenazy, Y., Bergamasco, A., Cardin, V., Carniel, S., D'Ortenzio, F., Garcia-Ladona, E., Garcia-Lafuente, J.M., Gogou, A., Gregoire, M., Hainbucher, D., Kontoyannis, H., Kovacevic, V., Krasakapoulou, E., Krokos, G., Incarbona, a, Mazzocchi, M.G., Orlic, M., Pascual, A., Poulain, P.-M., Rubino, A., Siokou-Frangou, J., Souvermezoglou, E., Sprovieri, M., Taupier-Letage, I., Tintoré, J., Triantafyllou, G., 2013. Physical forcing and physical/biochemical variability of the Mediterranean Sea: a review of unresolved issues and directions for future research. Ocean Sci. Discuss. 10, 1205–1280.
Marañón, E., Holligan, P., Varela, M., 2000. Basin-scale variability of phytoplankton biomass, production and growth in the Atlantic Ocean. Deep-Sea Res. I 47, 825–857.
Marañón, E., Behrenfeld, M., González, N., Mouriño, B., Zubkov, M., 2003. High variability of primary production in oligotrophic waters of the Atlantic Ocean: uncoupling from phytoplankton biomass and size structure. Mar. Ecol. Prog. Ser. 257, 1–11.
Marra, J., 2009. Net and gross productivity: weighing in with 14C. Aquat. Microb. Ecol. 56, 123–131.
Morán, X.A.G., Estrada, M., 2001. Short-term variability of photosynthetic parameters and particulate and dissolved primary production in the Alboran Sea (SW Mediterranean). Mar. Ecol. Prog. Ser. 212, 53–67.
Navarro, G., Ruiz, J., 2006. Spatial and temporal variability of phytoplankton in the Gulf of Cádiz through remote sensing images. Deep-Sea Res. II 53, 1241–1260.
Navarro, G., Ruiz, J., Huertas, I., Garcia, C., Criadoaldeanueva, F., Echevarria, F., 2006. Basin-scale structures governing the position of the deep fluorescence maximum in the Gulf of Cádiz. Deep-Sea Res. II 53, 1261–1281.
Navarro, G., Caballero, I., Prieto, L., 2012. Seasonal-to-interannual variability of chlorophyll – a bloom timing associated with physical forcing in the Gulf of Cádiz. Adv. Space Res. 50, 1164–1172.
Oguz, T., Macías, D., Renault, L., Ruiz, J., Tintore, J., 2013. Controls of plankton production by pelagic fish predation and resource availability in the Alboran and Balearic Seas. Prog. Oceanogr. 112–113, 1–14.
Platt, T., Sathyendranath, S., Ravindran, P., 1990. Primary production by phytoplankton: analytic solutions for daily rates per unit area of water surface. Proc. R. Soc. B 241, 101–111.
Quevedo, M., Anadón, R., 2001. Protist control of phytoplankton growth in the subtropical north-east Atlantic. Mar. Ecol. Prog. Ser. 221, 29–38.
Ramírez-Romero, E., Macías, D., Bruno, M., Reyes, E., Navarro, G., García, C.M., 2012. Submesoscale, tidally-induced biogeochemical patterns in the Strait of Gibraltar. Estuar. Coast. Shelf Sci. 101, 24–32.
Ramírez-Romero, E., Macías, D., García, C.M., Bruno, M., 2014. Biogeochemical patterns in the Atlantic Inflow through the Strait of Gibraltar. Deep-Sea Res. I Oceanogr. Res. Pap. 85, 88–100.
Reul, A., Vargas, J., Jimenez-Gomez, F., Echevarria, F., Garcia-Lafuente, J., Rodriguez, J., 2002. Exchange of planktonic biomass through the Strait of Gibraltar in late summer conditions. Deep-Sea Res. II 49, 4131–4144.
Reul, A., Rodríguez, V., Jimenez-Gomez, F., Blanco, J.M., Bautista, B., Sarhan, T., Guerrero, F., Ruiz, J., Garcia-Lafuente, J., 2005. Variability in the spatio-temporal distribution and size-structure of phytoplankton across an upwelling area in the NW-Alboran Sea,(W-Mediterranean). Cont. Shelf Res. 25, 589–608.
Reul, A., Muñoz, M., Criado-Aldeanueva, F., Rodriguez, V., 2006. Spatial distribution of phytoplankton <13 μm in the Gulf of Cádiz in relation to water masses and circulation pattern under westerly and easterly wind regimes. Deep-Sea Res. II 53, 1294–1313.
Reul, A., Rodríguez, J., Guerrero, F., González, N., Vargas, J., Echevarría, F., Rodríguez, V., Jiménez-Gómez, F., 2008. Distribution and size biomass structure of nanophytoplankton in the Strait of Gibraltar. Aquat. Microb. Ecol. 52, 253–262.
Robinson, C., Tilstone, G., Rees, A., Smyth, T., Fishwick, J., Tarran, G., Luz, B., Barkan, E., David, E., 2009. Comparison of in vitro and in situ plankton production determinations. Aquat. Microb. Ecol. 54, 13–34.
Sakshaug, E., Bricaud, A., Dandonneau, Y., Falkowski, P.G., Kiefer, D., Legendre, L., Morel, A., Parslow, J., Takahashi, M., 1997. Parameters of photosynthesis: definitions, theory and interpretation of results. J. Plankton Res. 19, 1637–1670.
Sánchez-Garrido, J.C., Sannino, G., Liberti, L., García Lafuente, J., Pratt, L., 2011. Numerical modeling of three-dimensional stratified tidal flow over Camarinal Sill, Strait of Gibraltar. J. Geophys. Res. 116, 1–17.
Sannino, G., Carillo, A., Artale, V., 2007. Three-layer view of transports and hydraulics in the Strait of Gibraltar: A three-dimensional model study. J. Geophys. Res. 112 (C3).
Sannino, G., Herrmann, M., Carillo, a., Rupolo, V., Ruggiero, V., Artale, V., Heimbach, P., 2009. An eddy-permitting model of the Mediterranean Sea with a two-way grid refinement at the Strait of Gibraltar. Ocean Model 30, 56–72.
Sarhan, T., Garcia-Lafuente, J., Vargas, M., Vargas, J.M., Plaza, F., 2000. Upwelling mechanisms in the northwestern Alboran Sea. J. Mar. Syst. 23, 317–331.
Siokou-Frangou, I., Christaki, U., Mazzocchi, M.G., Montresor, M., Ribera d'Alcalá, M., Vaqué, D., Zingone, a., 2010. Plankton in the open Mediterranean Sea: a review. Biogeosciences 7, 1543–1586.
Skliris, N., Beckers, J., 2009. Modelling the Gibraltar Strait/Western Alboran Sea ecohydrodynamics. Ocean Dyn. 59, 489–508.
Smith, S.D., Dobson, F.W., 1984. The heat budget at ocean weather station Bravo. Atmos. Ocean. 22, 1–22.
Sverdrup, H., 1953. On conditions for the vernal blooming of phytoplankton. J. Cons. Int. Explor. Mer 287–295.
Taylor, A., Geider, R., Gilbert, F., 1997. Seasonal and latitudinal dependencies of phytoplankton carbon-to-chlorophyll a ratios: results of a modelling study. Mar. Ecol. Prog. Ser. 152, 51–66.
Taylor, A., Harbour, D., Harris, R.P., Burkill, P.H., ES, E., 1993. Seasonal succession in the pelagic ecosystem of the North Atlantic and the utilization of nitrogen. J. Plankton Res. 15, 875–891.
Teira, E., Mourino, B., Marañón, E., Perez, V., Pazo, M., Serret, P., Dearmas, D., Escanez, J., Woodward, E., Fernandez, E., 2005. Variability of chlorophyll and primary production in the Eastern North Atlantic Subtropical Gyre: potential factors affecting phytoplankton activity. Deep-Sea Res. I 52, 569–588.

Toro, E.F., 1989. A weighted average flux method for hyperbolic conservation laws. Proc. R. Soc. Lond. A Math. Phys. 423, 401–418.
Vázquez, A., Bruno, M., Izquierdo, A., Macías, D., Ruiz-Cañavate, A., 2008. Meteorologically forced subinertial flows and internal wave generation at the main sill of the Strait of Gibraltar. Deep-Sea Res. I 55, 1277–1283.
Vázquez, A., Flecha, S., Bruno, M., Macías, D., Navarro, G., 2009. Internal waves and short-scale distribution patterns of chlorophyll in the Strait of Gibraltar and Alborán Sea. Geophys. Res. Lett. 36, 1–6.
Vichi, M., Masina, S., 2009. Skill assessment of the PELAGOS global ocean biogeochemistry model over the period 1980–2000. Biogeosciences 6, 2333–2353.
Vichi, M., Masina, S., Navarra, A., 2007a. A generalized model of pelagic biogeochemistry for the global ocean ecosystem. Part II: Numerical simulations. J. Mar. Syst. 64, 110–134.
Vichi, M., Pinardi, N., Masina, S., 2007b. A generalized model of pelagic biogeochemistry for the global ocean ecosystem. Part I: Theory. J. Mar. Syst. 64, 89–109.
Wesson, J., Gregg, M., 1994. Mixing at Camarinal sill in the Strait of Gibraltar. J. Geophys. Res. 99, 9847–9878.